



Nanoscale

Assembly Mechanism of Surface-Functionalized Nanocubes

| | |
|-------------------------------|---|
| Journal: | <i>Nanoscale</i> |
| Manuscript ID | NR-ART-12-2021-007995.R1 |
| Article Type: | Paper |
| Date Submitted by the Author: | 16-Feb-2022 |
| Complete List of Authors: | Lee, Brian; Duke University, Mechanical Engineering and Materials Science Arya, Gaurav; Duke University, Mechanical Engineering & Materials Science; Duke University |
| | |

SCHOLARONE™
Manuscripts

Assembly Mechanism of Surface-Functionalized Nanocubes

Brian Hyun-jong Lee and Gaurav Arya*

*Department of Mechanical Engineering and Material Science,
Duke University, Durham, NC 27708, USA*

E-mail: gaurav.arya@duke.edu

Phone: +1 (919) 660-5435. Fax: +1 (919) 660-8963

Abstract

Faceted nanoparticles can be used as building blocks to assemble nanomaterials with exceptional optical and catalytic properties. Recent studies have shown that surface functionalization of such nanoparticles with organic molecules, polymer chains, or DNA can be used to control the separation distance and orientation of particles within their assemblies. In this study, we computationally investigate the mechanism of assembly of nanocubes grafted with short-chain molecules. Our approach involves computing the interaction free energy landscape of a pair of such nanocubes via Monte Carlo simulations and using the Dijkstra algorithm to determine the minimum free energy pathway connecting key states in the landscape. We find that the assembly pathway of nanocubes is very rugged involving multiple energy barriers and metastable states. Analysis of nanocube configurations along the pathway reveals that the assembly mechanism is dominated by sliding motion of nanocubes relative to each other punctuated by their local dissociation at grafting points involving lineal separation and rolling motions. The height of energy barriers between metastable states depends on factors such as the interaction strength and surface roughness of the nanocubes and the steric repulsion from the grafts. These results imply that the observed assembly configuration of nanocubes depends not only on their globally stable minimum free energy state but also on the assembly pathway leading to this state. The free energy landscapes and assembly pathways presented in this study along with the proposed guidelines for engineering such pathways should be useful to researchers aiming to achieve uniform nanostructures from self-assembly of faceted nanoparticles.

INTRODUCTION

Self-assembly of faceted nanoparticles (NPs) offers an attractive approach for fabricating unique and complex nanostructures.¹⁻⁷ In cases where these NPs are made of noble metals, the NP assemblies can exhibit intriguing plasmonic, optical, and catalytic properties that are highly sensitive to the local arrangement of NPs within the structure.^{1-3,8-10} Hence, controlling both the translational and rotational order of faceted NPs within their higher-order assemblies is crucial for creating the next generation of nanodevices and materials with desired properties. A simple yet versatile strategy for inducing NPs into specific interparticle distances and orientations involves grafting of ligands such as polymer chains, organic molecules, or DNA onto the NP surfaces.¹⁻⁴ While bare NPs, especially those made of materials with large Hamaker constants, tend to assemble into close-packed structures with face-face contacts so as to maximize attractive van der Waals (vdW) interactions between particles, surface functionalization induces the formation of more open structures with spaced out or slanted faces that reduces the confinement of the grafted ligands between the NP surfaces, leading to lower steric repulsion between the grafts. By modulating this competition between vdW and steric forces through factors such as the length and chemistry of the tethered molecules, the size and material of the NPs, and solvent quality,¹⁻⁵ experiments have successfully assembled NP structures with exceptional properties such as plasmonic hotspots^{1,11,12} and orientationally disordered crystals.^{13,14}

Recently, we investigated the assembly behavior of nanocubes grafted with short-chain molecules. In particular, we used Monte Carlo simulations to compute the free energy landscape of a pair of surface-functionalized nanocubes treated using a coarse-grained model.¹⁵ Analyses of the minimum free energy (MFE) configurations obtained from these landscape revealed that the nanocubes exhibit one of three possible globally stable configurations (“phases”), namely the edge-edge, face-face, and intermediate phases that are distinguished by the amount of grafted ligands they enclose between their apposing faces. Additionally, based on how the MFE configuration varied with certain material parameters, we were able

to build a comprehensive phase diagram of nanocube configurations in this parameter space. While the simulations correctly predicted and explained many of the experimentally observed interparticle configurations in assemblies of polymer-grafted nanocubes, two important aspects of the assembly mechanism were not addressed. First, experiments have demonstrated that nanocubes do not assemble into a single configuration but exhibit multiple different configurations.¹⁻³ This suggests that not all of the nanocubes may have assembled into their global MFE or stable configuration and that some may have assembled into local MFE or metastable configurations. Second, some experiments have reported that nanocubes which initially assemble into edge-edge configurations transitioned into face-face configurations after they were thermally annealed.¹ This implies that, while the face-face configuration was the more energetically favored state, the nanocubes first assembled into a metastable edge-edge state and required higher thermal energy to transition into their globally stable state. Both sets of experimental results suggest that a full understanding of the metastable configurations exhibited by our nanocubes and the mechanism of transition between these states is crucial for controlling the assembled configurations of faceted NPs.

The task of identifying metastable states and determining transition pathways is not trivial, as the configurational free energy landscape of anisotropic NPs, even a pair of them, is multidimensional. This is in sharp contrast to spherical NPs whose pairwise interactions can be fully described by a single coordinate, the separation distance between NPs. This difficulty can be overcome through the minimum free energy pathway (MFEP) analysis commonly employed in biophysics to understand how proteins undergo functionally relevant transitions across metastable and stable states. While a pair of such states can be connected by an infinite number of pathways, there usually exists a unique pathway which minimizes the path-integral of free energy amongst all possible pathways. This pathway, termed the MFEP, represents the most probable pathway taken by the system to transition between the two states. By analyzing the conformational changes and the energetic barriers associated with this pathway, the kinetics and mechanism of the transition between two metastable

states or between a metastable and a stable state can be obtained.

In this study, we employ our previously utilized simulation model of surface-functionalized nanocubes¹⁵ and undertake a free energy landscape based MFEP analysis to investigate the assembly mechanism of a pair of such nanocubes. Our results show that the two-particle interaction free energy landscapes are inhabited by multiple metastable states and that transitions between these states along the MFEPs incur large energy barriers, leading to unusually slow transition rates. We find that the incorporation of surface roughness of nanocubes is required to reduce the heights of these barriers and bring the transition rates to within experimental time scales. Analysis of configurations along the MFEPs reveals that the nanocubes transition to their globally stable configurations through association and dissociation steps involving a combination of sliding, rolling, and lineal motions. Importantly, the MFEPs are able to explain the experimentally observed phenomena of nanocubes exhibiting a distribution of configurational states within assemblies and of thermal annealing inducing transitions from metastable to stable states.

COMPUTATIONAL METHODS

System configuration. The experimental system of interest consists of nanocubes embedded in a thin liquid film, where confinement and interfacial effects cause the NPs to lie flat and parallel to the air-liquid interface.¹⁻³ Thus, in our model, we assume that the nanocubes cannot exhibit translational or rotational motion in the z direction normal to the film surface. To describe the interparticle configuration of two nanocubes constrained to such quasi-2D environment, we consider that one of the nanocubes is at the origin with its facets parallel to the Cartesian axes and use the following three coordinates to describe the position and orientation of the other nanocube (Fig. 1a): the minimum distance of approach d_s between the surfaces of the nanocubes along the x axis, the lateral offset d_y of the nanocubes in the y axis, and the relative orientation θ of the nanocubes. This coordinate system was chosen as it conveniently represents the mechanism of nanocube assembly (see

Fig. 1b). For example, the association and dissociation of the nanocubes through a *sliding* motion can be completely described by changes in a single variable, d_y . Similarly, variations in d_s and θ represent *lineal* (head-on translation) and *rolling* motions, respectively.

Coarse-grained model. To obtain the interaction energy between the nanocubes in a computationally efficient manner, we utilized a simple coarse-grained model of surface-functionalized nanocubes employed in our previous study that captured sufficiently well the geometry and interactions of ligand-grafted nanocubes.¹⁵ Briefly, the nanocubes were treated as rigid bodies carved out of a simple cubic lattice of beads representing groups of atoms, and the grafted ligands were treated using a bead-spring model, where each bead represented a short segment of the ligand. In addition to these nanocubes that we termed ideal nanocubes, we also studied rough nanocubes with a topography consistent with that measured experimentally.¹⁶ These rough nanocubes were modeled by attaching an extra 24% surface beads at random positions on each face of the nanocubes. All beads in the system interact with each other *via* the Lennard Jones (LJ) potential $U_{\text{LJ}} = 4\varepsilon_{ij} [(\sigma_{ij}/r_{ij})^{12} - (\sigma_{ij}/r_{ij})^6]$, where ε_{ij} , σ_{ij} , and r_{ij} represent the LJ energy and size parameters and the separation distance of the interacting beads i and j . The intramolecular interactions of the tethered chains were described by harmonic bond stretching and bending potentials $U_s = \frac{1}{2}k_s(l - l_0)^2$ and $U_b = \frac{1}{2}k_b(\theta - \theta_0)^2$, where k_s and k_b represent force constants, l and θ the bond length and angle, and l_0 and θ_0 their corresponding equilibrium values. The ligands were attached to each nanocube face in a square pattern, also *via* harmonic springs of parameters k_s and l_0 . The solvent molecules were treated implicitly and their effects on the interaction between nanocubes is embedded in the interaction parameters ε_{ij} of the ligands and nanocubes. We note that our model accounts only for weak vdW interactions and steric hindrance between ligands and is not suitable for nanocubes grafted with ligands exhibiting strong attractive interactions, such as hydrogen bonding, π - π stacking, or electrostatic interactions. Experiments^{4,6,17} and simulations¹⁸ on DNA-grafted NPs, where such interactions play a larger role, have shown that they exhibit novel assembly behavior including reconfigurable or chiral

nanostructures that cannot be captured by our model.

Following previous work,¹⁵ the LJ size parameter σ_{cc} for interactions between nanocubes was set equal to 0.4σ and the nanocube side length $D = 10\sigma$, where σ represents an arbitrary length scale. The LJ energy parameter ε_{cc} was varied between 0.25 to 3ε to probe the role of vdW interactions, where ε represents an arbitrary energy scale. Unless indicated otherwise, we fixed the temperature to $T = \varepsilon/k_B$, where k_B is the Boltzmann constant; thus, ε effectively varies between 0.25 to $3k_B T$. The LJ size parameter σ_{lig} for ligand-ligand interactions was varied between 0.25 to 1σ to probe the effects of ligand segment excluded volume, and l_0 and θ_0 were set equal to σ_{lig} and 180° . The LJ size parameter σ_{lc} for the interactions between nanocube and ligand beads was obtained using the Lorentz-Berthelot mixing rule:¹⁹ $\sigma_{lc} = (\sigma_{cc} + \sigma_{lig})/2$. The LJ energy parameters ε_{lig} and ε_{lc} for ligand-ligand and ligand-nanocube interactions were kept fixed at 0.1ε to model weak interactions mediated by the ligands in good solvent.¹⁻³ To reduce computational cost, we employed a cutoff distance of 3σ for LJ interactions between ligands or those between ligands and nanocubes, as these interactions were calculated on the fly at each simulation step due to changing ligand conformations. However, no such cutoff was needed for LJ interactions between nanocube beads, which remained fixed during simulations and were therefore calculated only once before each simulation. The intramolecular force constants k_s and k_b were set equal to $10\varepsilon/\sigma$ and $0.1\varepsilon/\text{rad}^2$ to describe flexible chains. The length L and grafting density Γ of the ligands were fixed to 4 beads and 0.04 chains/ σ^2 to model short chains to ensure that the steric repulsion between chains remains weaker than the vdW interactions to allow the nanocube assembly. A detailed description of the model is provided elsewhere.¹⁵

Minimum free energy pathway. The MFEPs were obtained through the steps illustrated in Fig. 1d. First, we calculated the free energy landscape $F \equiv F(d_s, d_y, \theta)$, which is essentially the potential of mean force (PMF) of two nanocubes obtained as a function of their interparticle configuration. To obtain the PMF, we first computed $\langle f_x(d_s, d_y, \theta) \rangle$, the ensemble average of the x -component force acting between the two nanocubes, at all

separation distances d_s within a cutoff distance of d_{cut} where the force has decayed to zero. To compute these forces, the nanocubes were held fixed at each configuration while ligand conformations were sampled through configurational-bias Monte Carlo methods.²⁰ The forces were then integrated according to $F(d_s, d_y, \theta) = -\int_{d_{\text{cut}}}^{d_s} \langle f_x(\xi, d_y, \theta) \rangle d\xi$ to obtain the PMF. The free energy landscape was obtained for the range $d_s \in (0, 8\sigma)$, $d_y \in (0, 10\sigma)$, and $\theta \in (0^\circ, 45^\circ)$ at a resolution of $0.1\sigma \times 0.4\sigma \times 1^\circ$. We refer readers to our previous study for more detailed explanation of this procedure.¹⁵

Next, we located the minima in this free energy landscape corresponding to the phases reported earlier.¹⁵ In particular, we showed that nanocubes can assemble into three types of configurations — face-face (*FF*), intermediate (*I*), or edge-edge (*EE*) states — depending on the amount of ligands enclosed by the interacting faces of the nanocubes. Specifically, the *FF*, *I*, and *EE* states represent nanocubes that confine all, a fraction, or none of the ligands, respectively. In the coordinate system employed in this study (Fig. 1a), these phases are captured well by a single variable, d_y : configurations with $d_y \geq 0.75D$ for $\Gamma = 0.04/\sigma^2$ nanocubes are in the *FF* state as they lead to all of the grafted ligands being enclosed by the interacting surfaces of the nanocubes; configurations with $0.75D > d_y \geq 0.25D$ belong to the *I* state; and those with $d_y < 0.25D$ are in the *EE* state as the interacting faces do not confine any ligand. Therefore, to obtain the energetically stable configuration of the nanocubes for each phase, we identified the local free energy minimum within these specified d_y bounds corresponding to each of the three phases.

Lastly, the MFEPs between the identified free energy minima were obtained by finding the path of least action²¹ connecting the minima. In general, such pathways are obtained either through chain-of-states type of methods, such as nudged elastic band^{22,23} or string²⁴ methods, or algorithms based on graph theory.^{25–29} For this study, the graph theory approach was used as it is more appropriate for extracting the MFEP from a pre-computed free energy landscape. Specifically, we treat the free-energy landscape as a weighted network in which each configuration is represented as a node that is connected to its adjacent nodes (i.e.,

configurations at the adjacent grid point in either d_s , d_y , or θ) with weights equal to the differences in their free energies. The MFEPs were then computed by finding the shortest paths between the nodes corresponding to the local MFE configurations through the Dijkstra algorithm implemented in MATLAB.^{30,31}

Reaction coordinate and transition rates. To facilitate analysis of the MFEPs, we defined a reaction coordinate that represents the MFEP as a 1D pathway. In this reaction coordinate, changes in nanocube configuration due to the different modes of displacement (d_s , d_y , or θ) are equalized in terms of the cumulative distance by which the atoms of the nanocube get displaced *via* each mode (Fig. 1c). For instance, a Δd_s change in separation distance between the nanocubes would lead to a cumulative displacement of $n_{\text{atom}}\Delta d_s$, where n_{atom} is the number of atoms in the nanocube. Similarly, rotation of the nanocubes by an angle $\Delta\theta$ would lead to a cumulative displacement of $\Delta\theta \sum_{\text{atom}} r_{\text{atom}}$ equal to the sum of the arc lengths travelled by all atoms, where r_{atom} is the radial distance of each atom from the nanocube center along the x - y plane. Using this definition, the reaction coordinate which we denote by χ is given by the cumulative distance travelled by the nanocube atoms due to changes in nanocube configuration as they progress through the MFEP starting from a suitable initial configuration:

$$\chi \equiv \frac{\sum_{i \in \text{MFEP}} (n_{\text{atom}}|\Delta d_{s,i}| + n_{\text{atom}}|\Delta d_{y,i}| + |\Delta\theta_i| \sum_{\text{atom}} r_{\text{atom}})}{n_{\text{atom}}D}. \quad (1)$$

Here, the outer summation runs over the traversed nanocube configurations and the cumulative distance is normalized by $n_{\text{atom}}D$ so that nanocubes undergoing transition from a tip-to-tip to a *FF* configuration through purely sliding motion would lead to a reaction coordinate value of 1.

The transition rates between the free energy minima in the MFEPs were obtained using Kramers' theory, which provides a closed-form solution to the rate of escape of a thermally equilibrated system over an energy barrier.^{32,33} The theory is applicable when the system

dynamics are well described by a 1D free energy landscape and the energy barrier is much larger than thermal energy $k_B T$. If the position-dependent free energies of the system along coordinate x is given by $F(x)$, the barrier crossing rate k from one energy minimum to another is given by

$$k = \frac{\sqrt{F''(x_{\min})|F''(x_{\max})|}}{2\pi\gamma} \exp(-\Delta F/k_B T), \quad (2)$$

where x_{\min} and x_{\max} are the positions of the free energy minimum and barrier along the reaction coordinate, $\Delta F \equiv F(x_{\max}) - F(x_{\min})$ is the barrier height, and $F'' \equiv d^2 F/dx^2$ is the curvature of the free energy landscape computed through second-order central finite differences. γ represents the friction constant, which was calculated as $\gamma = 1.384 \times 3\pi\eta D$ according to the translational friction factor of cube-shaped particles.³⁴ The solvent viscosity η was assumed to be that of water at room temperature, i.e., 0.89 mPa·s.

RESULTS AND DISCUSSION

Assembly mechanism of bare nanocubes. As a first step to understanding the assembly pathway of surface-functionalized nanocubes, we studied the assembly behavior of bare nanocubes. The absence of ligand interactions makes this system a good control for dissecting the role of vdW interactions acting between the particle cores of surface-functionalized NPs in their assembly. The free energy landscape computed for bare nanocubes is depicted in Fig. 2a and it reveals that their free energy F is negligible across the vast majority of the configurational space compared to its value at the FF configuration ($d_s = 0$, $d_y = D$, $\theta = 0^\circ$) representing the global minimum in the landscape. This is even more apparent in the 2D representations of the 3D landscape shown in Fig. 2b and Fig. 2c, where the portrayed energies represent F values at the indicated two coordinate values minimized with respect to the third coordinate; for instance, in Fig. 2b, we have plotted $F(d_y, \theta)$ at values of d_s that yield the lowest free energy at those (d_y, θ) . Both sets of results show that bare nanocubes assemble in the FF configuration and that their free energy decays sharply with deviations

from this configuration.

To gain insight into the assembly mechanism of bare nanocubes, we analyzed the free energy pathway of bare nanocubes as they transition from a dissociated state to the FF state, first purely through a *single* association mechanism (Fig. 2d). Specifically, the change in F through a purely lineal association (LA) mechanism was examined by varying d_s from D to 0 while the other two coordinates were kept fixed at $d_y = D$ and $\theta = 0^\circ$. The sliding association (SA) mechanism was probed by changing d_y from 0 to D with fixed $d_s = 0$ and $\theta = 0^\circ$. Lastly, the rolling association (RA) mechanism was examined by changing θ from 90° to 0° with $d_s = 0$ and $d_y = D$. To make the comparison of the three mechanisms more convenient, the changes in the configuration of the nanocubes are normalized so that the fully dissociated state has a value of 0 and the FF state a value of 1 in the normalized coordinate system. The results demonstrate that the magnitude of F increases linearly with respect to d_y throughout the SA mechanism. However, for both the RA and LA mechanisms, F is negligible for most configurations except near the FF configuration where the free energies change drastically. In addition, the energetic penalty for deviating from the FF configuration is greater through lineal motion than through rolling motion. This is because lineal dissociation (LD) involves dissociation of atoms across the entire surface of the nanocubes while rolling dissociation (RD) leads to separation of only a fraction of the atoms, as the atoms on the edges of the nanocubes remain associated.

In the above analysis, both the SA and RA mechanisms start from the same tip-to-tip configuration of nanocubes, but follow distinct paths towards the same FF configuration—the global MFE state of bare nanocubes. While the free energy profiles plotted in Fig. 2d clearly suggest that SA would be the favored pathway over RA, it is unclear if SA also is the MFEP between these two configurations. We therefore determined the MFEP between the tip-to-tip and FF configurations in the free energy landscape and found that the SA indeed represents the MFEP between the two states (see Fig. 2a).

Assembly mechanism of surface-functionalized nanocubes. As observed in our

previous study,¹⁵ surface-functionalized nanocubes exhibit stable FF , EE , and I states, with the globally stable (global MFE) state switching between the three states depending on the strength ε_{cc} of the vdW interactions between the nanocubes and the excluded volume σ_{lig} of the ligand segments (Fig. 3a). In particular, increasing σ_{lig} causes the nanocubes to transition from the FF to the I to the EE states, while increasing ε_{cc} causes the opposite sequence of transitions. We previously showed that these transitions occur because both the attractive vdW interactions between nanocubes and the repulsive steric interactions between ligands are the strongest for the FF state and the weakest for the EE state. This means that the FF state is energetically favored when the system is dominated by attractive interactions (large ε_{cc} and small σ_{lig}) and the EE state is favored when repulsive interactions dominate (small ε_{cc} and large σ_{lig}), while the I state is favored at intermediate conditions. Thus, to properly study the assembly pathway of surface-functionalized nanocubes, we examined nanocube systems with different vdW interaction strengths and ligand segment excluded volumes, as indicated by rectangles in Fig. 3a, which gave us access to all three varieties of nanocubes, i.e., FF -, I -, and EE -forming nanocubes. For MFEP analyses, we again chose the tip-to-tip configuration ($d_s = 0$, $d_y = 0$, $\theta = 0^\circ$) to be the initial state, as this was the configuration with the most favorable free energy among all the dissociated configurations shown in Fig. 2d. We then determined the MFEP from the tip-to-tip configuration to the local energy minimum state in the EE phase, then MFEP from EE to I , and finally the MFEP from I to FF .

We first examined nanocubes with weak vdW interactions ($\varepsilon_{cc} = 0.75\varepsilon$) that formed the FF phase when $\sigma_{lig} = 0.5\sigma$ (blue rectangle in Fig. 3a) and the EE phase when $\sigma_{lig} = 0.75\sigma$ (red rectangle). The free energy landscapes and MFEPs computed for these two systems are depicted in Figs. 3b and 3c. Compared to bare nanocubes (Fig. 2a), surface-functionalized nanocubes exhibit weaker attraction and more complex variations in free energy with respect to configuration, especially for nanocubes grafted with ligands of larger segments (Fig. 2c). Fig. 3d–f plot the progression of free energy and configuration of the nanocubes along the

MFEP of the *FF*-forming nanocubes, where $d_y/D < 0.25$ indicates the *EE* phase, $d_y/D \geq 0.75D$ signifies the *FF* phase, and $0.25 \leq d_y/D < 0.75D$ corresponds to the *I* phase. Similar to the assembly of bare nanocubes, the association mechanism involves mainly SA (Fig. 3e). As the nanocubes slide toward the *FF* configuration, the free energy varies almost linearly with respect to d_y . However, unlike bare nanocubes, the MFEP here harbors several energy barriers as the nanocubes transition from the *EE* to the *I* to the *FF* phase (Fig. 3d). To help understand the origin of these barriers, we inspected nanocube configurations at the energy barriers (transition states) and wells (metastable states), as shown in Fig. 3g. We can observe that the metastable states labelled 2 and 4 correspond to configurations in which the surfaces of the nanocubes attempt to maximize their interaction area ($\propto d_y$) in the *EE* and *I* phases without crossing over to the next phase. On the other hand, the transition states labelled 3 and 5 occur as the surfaces of the nanocubes dissociate from each other to incorporate more grafts. While such dissociation incurs large energy penalty, it is a necessary step for the nanocubes to transition from one phase to another. The results plotted in Fig. 3e indicate that the dissociation at the first transition state follows a largely LD mechanism. This is followed by a prolonged SA concluded by a small RA leading to the *I* phase with a face-edge contact. At the second transition state, the dissociation occurs via a combination of LD and RD, which brings the nanocube surfaces to a parallel configuration. This is then followed by another prolonged SA to the *FF* phase, the global MFE configuration.

The MFEP of the *EE*-forming nanocubes displays many similarities with that of the *FF*-forming nanocubes described above. In particular, the free energy along the MFEP (Fig. 3h) displays multiple energy wells and barriers, and the assembly mechanism is again dominated by SA interspersed with combinations of LD, RA, and RD motions (Figs. 3i and 3k). However, the nanocubes are less parallel and involve larger rolling motions compared to the *FF*-forming nanocubes (Fig. 3e). For example, the *EE*-forming nanocubes are parallel only in the *EE* state (labelled 2 in Fig. 3h–k) and remain in slanted configurations with face-edge contacts ($\theta > 0^\circ$ and $d_s = 0$) in contrast to the parallel, surface-separated ($\theta = 0^\circ$ and

$d_s > 0$) configurations observed for the *FF*-forming nanocubes in Fig. 3d. This distinction in the assembly mechanism arises because the rolling motion affects the edge atoms and the rest of the atoms of the nanocubes differently depending on σ_{lig} . As d_s is large when σ_{lig} is large, the gain in vdW interaction energy by atoms on the edge of the nanocube as the nanocubes transition from parallel to the slanted configuration is larger than the loss in vdW energy by the rest of the atoms on the interacting surfaces of the nanocubes. However, for *FF*-forming nanocubes where σ_{lig} is small, the vdW energy gained by the edge atoms is smaller and the energy loss by the rest of the surface atoms is larger. Thus, the degree of involvement of rolling and lineal mechanisms in the dissociation of the nanocubes depends on the strength of repulsive interactions mediated by the grafted ligands.

In addition to weakly interacting nanocubes, we also investigated the *FF*-forming ($\sigma_{\text{lig}} = 0.5\sigma$) and *I*-forming ($\sigma_{\text{lig}} = 0.75\sigma$) nanocubes with strong vdW interactions ($\varepsilon_{\text{cc}} = 2\varepsilon$) marked by purple rectangles in Fig. 3a. The shape of the free energy profile along the MFEP as well as the assembly mechanism of the *FF*-forming nanocubes with strong interactions shown in Fig. 4a–d are very similar to those with weak interactions depicted in Fig. 3d–g, except for two notable differences. First, the magnitude of free energies are obviously much larger in nanocubes with strong interactions. Second, no energy barrier exists between the *I* and *FF* states. This is because the vdW interactions are now even more dominant and the increased free volume available to the grafts from the rolling motion does not outweigh the reduction in vdW energy. Consequently, the nanocubes prefer to remain parallel throughout the transition from the *I* to the *FF* state.

Lastly, the *I*-forming nanocubes with strong vdW interactions also assemble similarly to *EE*-forming nanocubes with weak interactions, except that the the MFE state now is the *I* rather than the *EE* phase. This is clearly a result of the stronger vdW interactions being able to overcome the steric repulsion from the grafts enclosed between the nanocube surfaces in the *I* phase. Since vdW interactions dominate steric repulsion in these *I*-forming nanocubes, the free energy is also consistently larger in magnitude across the MFEP.

While we have compared the strongly and weakly interacting nanocubes by modifying ε_{cc} , the above results also provide insight into the effect of nanocube size on their assembly behavior. Experimentally, Klinkova et al. have shown that polystyrene-grafted silver nanocubes tend to form homogeneous FF structures when the particles are large ($D = 45$ nm) whereas they form less uniform configurations consisting mostly of I and EE configurations for smaller D (25 nm).³ Our previous calculations^{15,35} have shown the interaction free energy between nanocubes scales more sharply with size for the FF state ($\propto D^2$) compared to the I state ($\propto D$). Therefore, the larger the nanocube, the greater its preference for the FF configuration. In addition, because the interaction strengths are weaker for smaller nanocubes, the height of free-energy barriers between metastable states will also be reduced, resulting in less uniform configurations for smaller nanocubes.

Effect of surface roughness. While the MFEPs presented in Figs. 3 and 4 provide useful insights into the assembly mechanism of surface-functionalized nanocubes, the predicted energy barriers between metastable states are $O(100k_B T)$. As most assembly experiments, such as those involving Ag nanocubes,^{1,2} are conducted at temperatures of 270–400 K and over time scales of hours, the large barriers imply that the nanocubes would not be able to transition between different stable phases within observable time scales. While this result could well be valid for many experimental cases in which thermal annealing does not alter the assembly configuration of nanocubes, it cannot explain the thermally-induced transition from EE to FF phases observed by Gao et al.¹ One possible cause of this discrepancy could be the overestimation of the vdW interaction energy between nanocubes due to our assumption of “ideal” nanocubes. In particular, our model assumes that the nanocubes are defectless, so their surfaces are atomically smooth. However, atomic force microscope imaging of Ag nanocubes revealed that their surface is not perfectly flat but has a root mean squared deviation of one to two atomic diameters.¹⁶ Such surface roughness can lead to a drastic reduction in the vdW interactions energy between faceted NPs as only a fraction of the surface atoms can be in contact with the other NP. Indeed, computational studies have

shown that NPs transition from an associated percolating gel to a dissociated fluid phase when surface roughness is incorporated.³⁶

To investigate the effects of roughness, we also obtained the MFEP of atomically corrugated “rough” nanocubes as introduced earlier. Fig. 5 presents the results obtained for such nanocubes with parameters ($\sigma_{\text{lig}} = 0.5\sigma$, $\varepsilon_{\text{cc}} = 0.75\varepsilon$) and ($\sigma_{\text{lig}} = 0.5\sigma$, $\varepsilon_{\text{cc}} = 2\varepsilon$), which lead to the *FF* phase in case of ideal nanocubes (see Fig. 3a). Similar to the MFEP of ideal nanocubes, the *FF* phase is the global MFE state for rough nanocubes. The mechanism of assembly from the *I* phase (labelled 3 in Figs. 5d and 5h) to the *FF* phase (labelled 4) also is dominated mostly by the SA mechanism. Furthermore, as was the case with ideal nanocubes, the assembly mechanism is very similar between rough nanocubes with large and small ε_{cc} .

However, two key differences emerge between the MFEPs of rough and ideal nanocubes. First, the overall magnitude of the free energy of rough nanocubes is $\approx 30\%$ of that of ideal nanocubes. Consequentially, the energy barriers between different states are also significantly smaller. For example, for the MFEP obtained with parameters of ($\sigma_{\text{lig}} = 0.5\sigma$, $\varepsilon_{\text{cc}} = 0.75\varepsilon$), the energy barrier between the *EE* and the *I* phase is $\approx 25k_{\text{B}}T$ (Fig. 5a) while it is $\approx 115k_{\text{B}}T$ for ideal nanocubes (Fig. 3d). Second, the assembly mechanism of rough nanocubes involves much more lineal and rolling motions. This is because the energy loss of the nanocubes from LD and RD is greatly reduced as less number of atoms are in contact with each other due to surface roughness.

A consequence of reduced interaction energies between nanocubes is that the kinetics of many of the transitions across phases are now within experimental time scales. In fact, using Kramer’s theory we can estimate the rate of transition from the *EE* to the *I* phase (labelled 1 \rightarrow 2 in Fig. 5c) for rough nanocubes with $\varepsilon_{\text{cc}} = 0.75\varepsilon$ at $T = 1\varepsilon/k_{\text{B}}$ to be $O(10^{-4}/s)$, indicating that this transition now occurs within experimental time scales. On the other hand, the rate of the *I* \rightarrow *FF* transition (labelled 3 \rightarrow 4) is $O(10^{-7}/s)$, indicating that the probability of this transition occurring within experimental time scales is still very low.

However, these results change drastically when thermal annealing is applied, for instance, when T is increased to $1.5\varepsilon/k_B$, which is equivalent to changing the temperature from 270 K to 400 K in experiments. Now, the transition rates between all three phases are larger than $O(10^{-5}/s)$. Therefore, the nanocubes are expected to spontaneously assemble into their global MFE configuration, the FF phase, within experimental time scales. In contrast, the transition rate for rough nanocubes with $\varepsilon_{cc} = 2\varepsilon$ are all less than $O(10^{-10}/s)$, indicating that a large fraction of these nanocubes are likely to be observed trapped in one or more of its metastable states (Fig. 5g). From these results, one can infer that the thermally-induced $EE \rightarrow FF$ transition experimentally observed by Gao et al.¹ likely belongs to the case where the energy barriers are such that thermal annealing is necessary for the transition to take place in experimental time scales, similar to the computational results shown in Fig. 5c.

CONCLUSIONS

We have computationally investigated the assembly mechanism of surface-functionalized nanocubes by carrying out MFEP analyses of their interaction free energy landscape. Our results show that the nanocubes exhibit multiple metastable states related to the FF , I , and EE phases reported earlier, and that the MFEP connecting these metastable states contains transition states with large free energy barriers. Analysis of nanocube configurations along the MFEP revealed that the transition between metastable states requires slight dissociation of the nanocubes, which allows them to incorporate more grafted ligands between their interacting faces. In general, the dissociation mechanism involves lineal separation of the nanocubes, while their ensuing progressive association towards the next metastable state follows a combination of sliding and rolling motions. In the future, it would be important to experimentally test these assembly pathway predictions using new, powerful spectroscopy techniques such as multimodal single-molecule FRET³⁷ and fluorescence correlation spectroscopy,³⁸ which can measure spatiotemporal changes in the relative location of fluorescent molecules strategically tagged onto the system of interest.

We also demonstrated that, similar to the globally stable state, the assembly pathway too is determined by the competition between attractive vdW interactions and repulsive steric interactions mediated by the nanocube cores and grafts, respectively. Specifically, increasing the strength of vdW interactions leads to more parallel configurations of the nanocubes and reduced rolling motions throughout the MFEP, whereas increasing the magnitude of steric interactions leads to more slanted configurations and pronounced rolling motions. Incorporation of surface roughness to the nanocubes greatly reduces the overall magnitude of vdW interactions between the nanocubes. Apart from making the lineal and rolling motions of the assembly pathway more pronounced, roughness leads to significant lowering of energy barriers that can cause some prohibitively slow transitions across metastable states to become more kinetically accessible. In some cases, thermal annealing is required to make transitions between metastable and stable states more kinetically accessible.

On the whole, this work suggests that the design of surface-functionalized NPs to target a specific assembly configuration needs to consider not only the globally stable state but also the MFEP leading to this state. For example, while our previous study¹⁵ suggested that strong attractive interactions between the nanocube cores will always lead to the *FF* state being favored, the results of this study indicate that the transition towards the *FF* state from the *I* or *EE* configurations might not occur within experimental time scales if the linear and rolling dissociative motions required between states incur large energetic penalties. Therefore, the interaction strength between the NPs needs to be adjusted so that the activation energy between metastable states is relatively weak while the energy well at the targeted configuration is much deeper compared to those of the metastable states. Such insights not only help explain the heterogeneity in interparticle configurations and thermally-induced transitions between them observed experimentally,¹⁻³ but they should also help engineer experimental systems that lead to more uniform assembly of nanocubes into targeted nanostructures.

ACKNOWLEDGMENTS

We thank Prof. Andrea Tao for valuable discussions. This work was sponsored in part by the National Science Foundation (Grant No. CMMI 1636356) and by the UC San Diego Materials Research Science and Engineering Center (UCSD MRSEC) supported by the National Science Foundation (Grant No. DMR-2011924). Computational resources were provided by the Duke Computing Cluster (DCC) and the Extreme Science and Engineering Discovery Environment (XSEDE) Program supported by the National Science Foundation (Grant No. ACI-1053575).

References

- (1) Gao, B.; Arya, G.; Tao, A. R. Self-orienting nanocubes for the assembly of plasmonic nanojunctions. *Nat. Nanotechnol.* **2012**, *7*, 433–437.
- (2) Gurunatha, K. L.; Marvi, S.; Arya, G.; Tao, A. R. Computationally Guided Assembly of Oriented Nanocubes by Modulating Grafted Polymer–Surface Interactions. *Nano Lett.* **2015**, *15*, 7377–7382.
- (3) Klinkova, A.; Thérien-Aubin, H.; Ahmed, A.; Nykypanchuk, D.; Choueiri, R. M.; Gagnon, B.; Muntyanu, A.; Gang, O.; Walker, G. C.; Kumacheva, E. Structural and optical properties of self-assembled chains of plasmonic nanocubes. *Nano Lett.* **2014**, *14*, 6314–6321.
- (4) Lu, F.; Vo, T.; Zhang, Y.; Frenkel, A.; Yager, K. G.; Kumar, S.; Gang, O. Unusual packing of soft-shelled nanocubes. *Sci. Adv.* **2019**, *5*, eaaw2399.
- (5) Quan, Z.; Xu, H.; Wang, C.; Wen, X.; Wang, Y.; Zhu, J.; Li, R.; Sheehan, C. J.; Wang, Z.; Smilgies, D.-M., et al. Solvent-mediated self-assembly of nanocube superlattices. *J. Am. Chem. Soc.* **2014**, *136*, 1352–1359.

- (6) O'Brien, M. N.; Girard, M.; Lin, H.-X.; Millan, J. A.; De La Cruz, M. O.; Lee, B.; Mirkin, C. A. Exploring the zone of anisotropy and broken symmetries in DNA-mediated nanoparticle crystallization. *Proc. Natl. Acad. Sci. USA* **2016**, *113*, 10485–10490.
- (7) Elbert, K. C.; Zygmunt, W.; Vo, T.; Vara, C. M.; Rosen, D. J.; Krook, N. M.; Glotzer, S. C.; Murray, C. B. Anisotropic nanocrystal shape and ligand design for co-assembly. *Sci. Adv.* **2021**, *7*, eabf9402.
- (8) Hsu, S.-W.; Rodarte, A. L.; Som, M.; Arya, G.; Tao, A. R. Colloidal plasmonic nanocomposites: from fabrication to optical function. *Chem. Rev.* **2018**, *118*, 3100–3120.
- (9) Clark, B. D.; Jacobson, C. R.; Lou, M.; Renard, D.; Wu, G.; Bursi, L.; Ali, A. S.; Swearer, D. F.; Tsai, A.-L.; Nordlander, P., et al. Aluminum nanocubes have sharp corners. *ACS Nano* **2019**, *13*, 9682–9691.
- (10) Das, R.; Sarkar, S. Optical properties of silver nano-cubes. *Opt. Mater.* **2015**, *48*, 203–208.
- (11) Gao, B.; Alvi, Y.; Rosen, D.; Lav, M.; Tao, A. R. Designer nanojunctions: orienting shaped nanoparticles within polymer thin-film nanocomposites. *Chem. Commun.* **2013**, *49*, 4382–4384.
- (12) Hooshmand, N.; Mousavi, H. S.; Panikkanvalappil, S. R.; Adibi, A.; El-Sayed, M. A. High-sensitivity molecular sensing using plasmonic nanocube chains in classical and quantum coupling regimes. *Nano Today* **2017**, *17*, 14–22.
- (13) Lee, Y. H.; Shi, W.; Yang, Y.; Kao, Y.-C.; Lee, H. K.; Chu, R.; Pang, Y. L.; Lay, C. L.; Li, S.; Ling, X. Y. Modulating Orientational Order to Organize Polyhedral Nanoparticles into Plastic Crystals and Uniform Metacrystals. *Angew. Chem.* **2020**, *132*, 21369–21375.

- (14) Knorowski, C.; Travasset, A. Self-Assembly and Crystallization of Hairy (f-Star) and DNA-Grafted Nanocubes. *J. Am. Chem. Soc.* **2014**, *136*, 653–659.
- (15) Lee, B. H.-j.; Arya, G. Orientational phase behavior of polymer-grafted nanocubes. *Nanoscale* **2019**, *11*, 15939–15957.
- (16) Xia, X.; Rycenga, M.; Qin, D.; Xia, Y. A silver nanocube on a gold microplate as a well-defined and highly active substrate for SERS detection. *J. Mater. Chem. C* **2013**, *1*, 6145–6150.
- (17) Sun, M.; Xu, L.; Bahng, J. H.; Kuang, H.; Alben, S.; Kotov, N. A.; Xu, C. Intracellular localization of nanoparticle dimers by chirality reversal. *Nat. Commun.* **2017**, *8*, 1–10.
- (18) Lee, B. H.-j.; Kotov, N. A.; Arya, G. Reconfigurable Chirality of DNA-Bridged Nanorod Dimers. *ACS Nano* **2021**, *15*, 13547–13558.
- (19) Rowlinson, J. S.; Swinton, F. L. *Liquids and liquid mixtures*; Butterworth-Heinemann, 1982.
- (20) Siepmann, J. I.; Frenkel, D. Configurational bias Monte Carlo: a new sampling scheme for flexible chains. *Mol. Phys.* **1992**, *75*, 59–70.
- (21) de Maupertuis, P. L. M. *Memoirs of the Royal Academy of Sciences of Paris*; Institut de France, 1744; pp 417–426.
- (22) Henkelman, G.; Uberuaga, B. P.; Jónsson, H. A climbing image nudged elastic band method for finding saddle points and minimum energy paths. *J. Chem. Phys.* **2000**, *113*, 9901–9904.
- (23) Trygubenko, S. A.; Wales, D. J. A doubly nudged elastic band method for finding transition states. *J. Chem. Phys.* **2004**, *120*, 2082–2094.
- (24) Weinan, E.; Ren, W.; Vanden-Eijnden, E. String method for the study of rare events. *Phys. Rev. B* **2002**, *66*, 052301.

- (25) Floyd, R. W. Algorithm 97: shortest path. *Commun. ACM* **1962**, *5*, 345.
- (26) Hart, P. E.; Nilsson, N. J.; Raphael, B. A formal basis for the heuristic determination of minimum cost paths. *IEEE Trans. Syst. Man Cybern. Syst.* **1968**, *4*, 100–107.
- (27) Cherkassky, B. V.; Goldberg, A. V.; Radzik, T. Shortest paths algorithms: Theory and experimental evaluation. *Math. Program.* **1996**, *73*, 129–174.
- (28) Marcos-Alcalde, I.; Setoain, J.; Mendieta-Moreno, J. I.; Mendieta, J.; Gómez-Puertas, P. MEPSA: minimum energy pathway analysis for energy landscapes. *Bioinformatics* **2015**, *31*, 3853–3855.
- (29) Seitz, E.; Frank, J. POLARIS: path of least action analysis on energy landscapes. *J. Chem. Inf. Model.* **2020**, *60*, 2581–2590.
- (30) Dijkstra, E. W. A note on two problems in connexion with graphs. *Numer. Math.* **1959**, *1*, 269–271.
- (31) Kirk, J. Dijkstra's Shortest Path Algorithm. <https://www.mathworks.com/matlabcentral/fileexchange/12850-dijkstra-s-shortest-path-algorithm>, 2021.
- (32) Kramers, H. A. Brownian motion in a field of force and the diffusion model of chemical reactions. *Physica* **1940**, *7*, 284–304.
- (33) Arya, G. Models for recovering the energy landscape of conformational transitions from single-molecule pulling experiments. *Mol. Simulat.* **2016**, *42*, 1102–1115.
- (34) Okada, K.; Satoh, A. Evaluation of the translational and rotational diffusion coefficients of a cubic particle (for the application to Brownian dynamics simulations). *Mol. Phys.* **2020**, *118*, e1631498.
- (35) Lee, B. H.-j.; Arya, G. Analytical van der Waals interaction potential for faceted nanoparticles. *Nanoscale Horiz.* **2020**, *5*, 1628–1642.

- (36) Olarte-Plata, J. D.; Brekke-Svaland, G.; Bresme, F. The influence of surface roughness on the adhesive interactions and phase behavior of suspensions of calcite nanoparticles. *Nanoscale* **2020**, *12*, 11165–11173.
- (37) Kilic, S.; Felekyan, S.; Doroshenko, O.; Boichenko, I.; Dimura, M.; Vardanyan, H.; Bryan, L. C.; Arya, G.; Seidel, C. A.; Fierz, B. Single-molecule FRET reveals multiscale chromatin dynamics modulated by HP1 α . *Nat. Commun.* **2018**, *9*, 1–14.
- (38) Song, J.-J.; Bhattacharya, R.; Kim, H.; Chang, J.; Tang, T.-Y.; Guo, H.; Ghosh, S. K.; Yang, Y.; Jiang, Z.; Kim, H., et al. One-dimensional anomalous diffusion of gold nanoparticles in a polymer melt. *Phys. Rev. Lett.* **2019**, *122*, 107802.

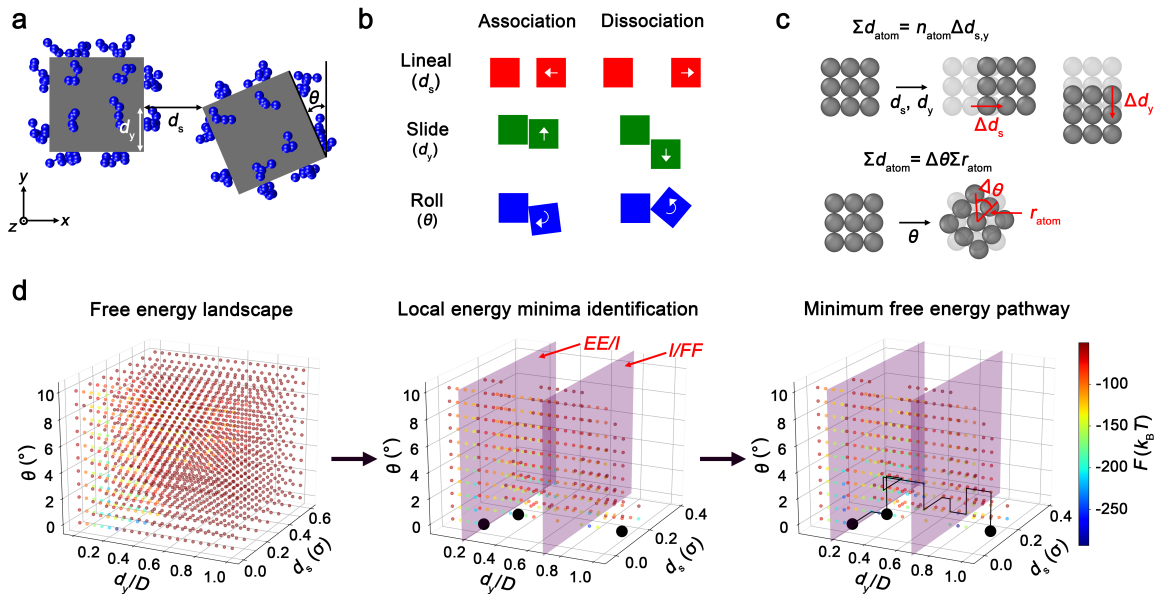


Figure 1: Schematics of the computational approach. (a) Coarse-grained model of surface-functionalized nanocubes with the coordinate system for describing their interparticle configuration. (b) Mechanism of nanocube association and dissociation involving lineal, sliding, and rolling motions. (c) Definition of the reaction coordinate based on total displacement of nanocube atoms. (d) Procedure for obtaining the MFEP, which involves computation of the free energy landscape, identification of the local energy minima corresponding to the *EE*, *I*, and *FF* phases, and determination of the MFEP by connecting local energy minima *via* the Dijkstra algorithm. Solid black circles represent the MFE configurations corresponding to the three phases and the purple planes represent boundaries between the three phase domains.

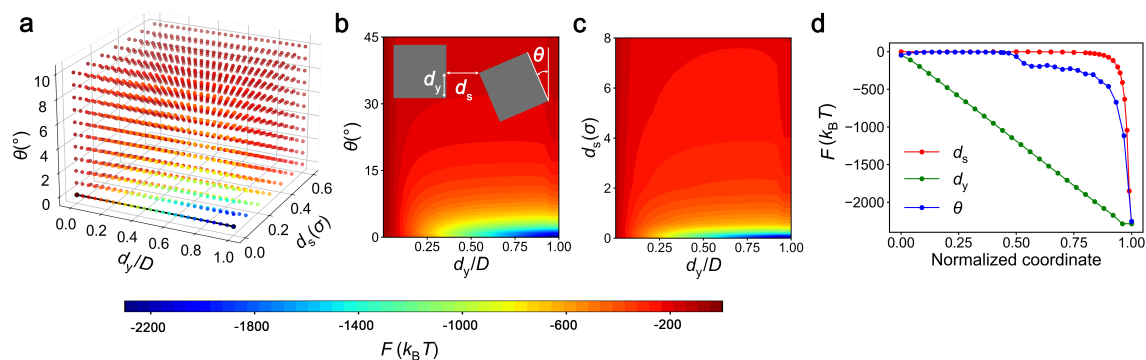
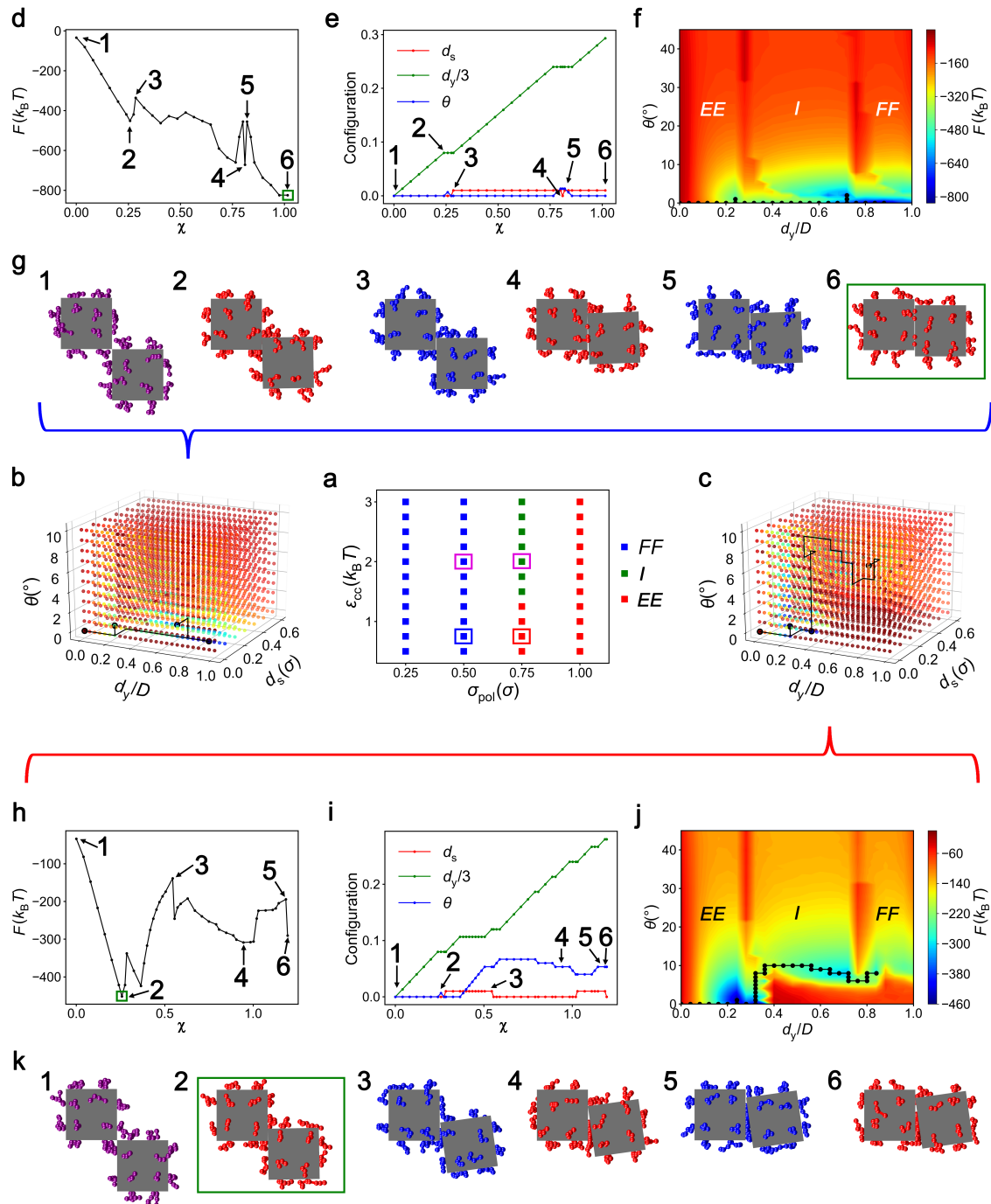


Figure 2: Assembly of bare nanocubes with $\varepsilon_{cc} = k_B T$. (a) Free energy landscape $F(d_s, d_y, \theta)$ showing the FF configuration as the global MFE state. The solid black line is the MFEP between the tip-to-tip and FF configurations depicted by solid black circles. (b) Free energy with respect to d_y and θ for values of d_s that minimize F . (c) Free energy with respect to d_y and d_s for values of θ that minimize F . (d) Free energy as nanocubes transition from the dissociated state to the ideal face-face state ($d_s = 0, d_y = D, \theta = 0^\circ$) with purely a single type of association mechanism. Color bar at the bottom applies to (a)–(c).



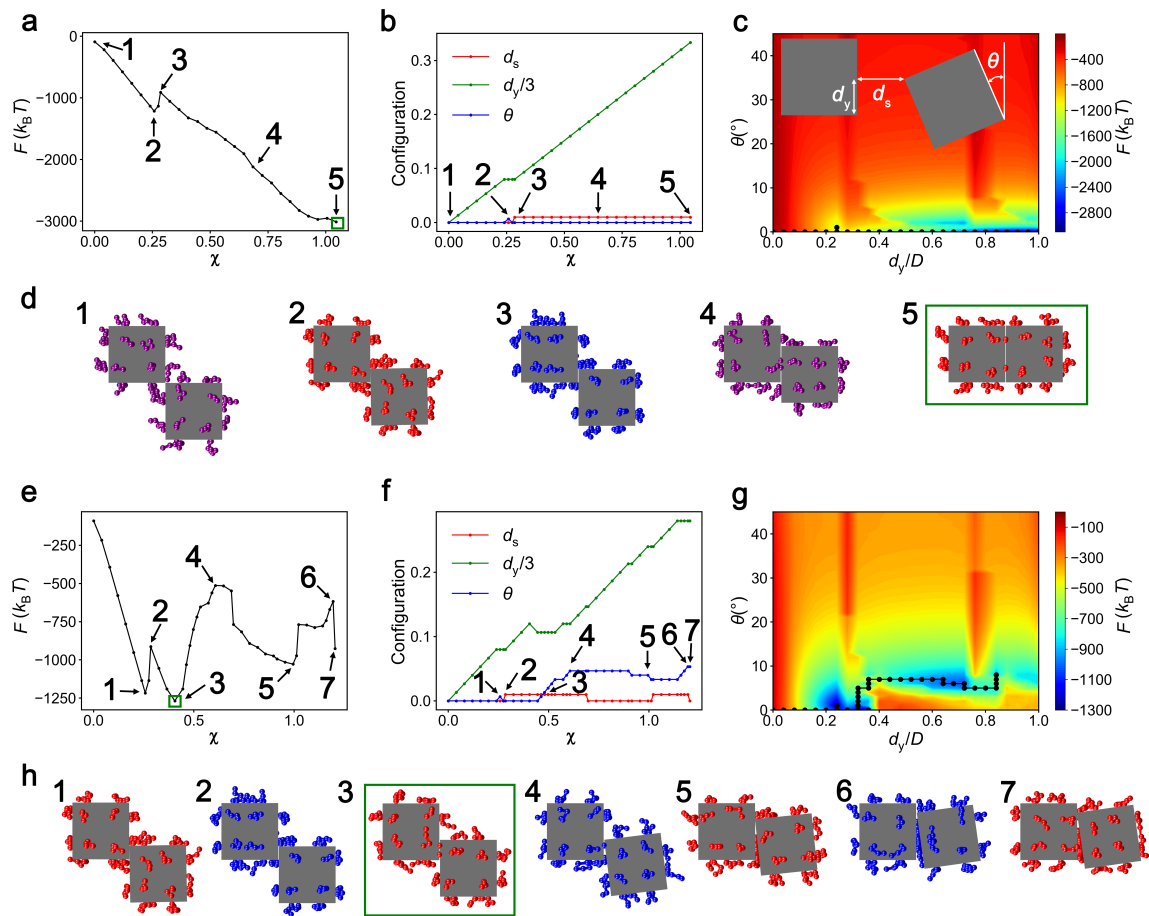


Figure 4: Assembly pathway of surface-functionalized nanocubes with strong vdW interactions. (a–h) Results corresponding to $[\sigma_{\text{lig}}, \varepsilon_{\text{cc}}] = [0.5\sigma, 2k_B T]$ (a–d) and $[0.75\sigma, 2k_B T]$ (e–h). (a, e) Free energy along the MFEP. (b, f) Nanocube configuration coordinates along the MFEP. (c, g) Free energy with respect to d_y and θ minimized with respect to d_s . (d, h) Representative nanocube configurations at specific points along the MFEP indicated in (a, e) and (b, f). Configurations at the tip-to-tip, metastable/stable, and transition states are distinguished by purple, red, and blue grafts. Green rectangle denotes the globally stable state.

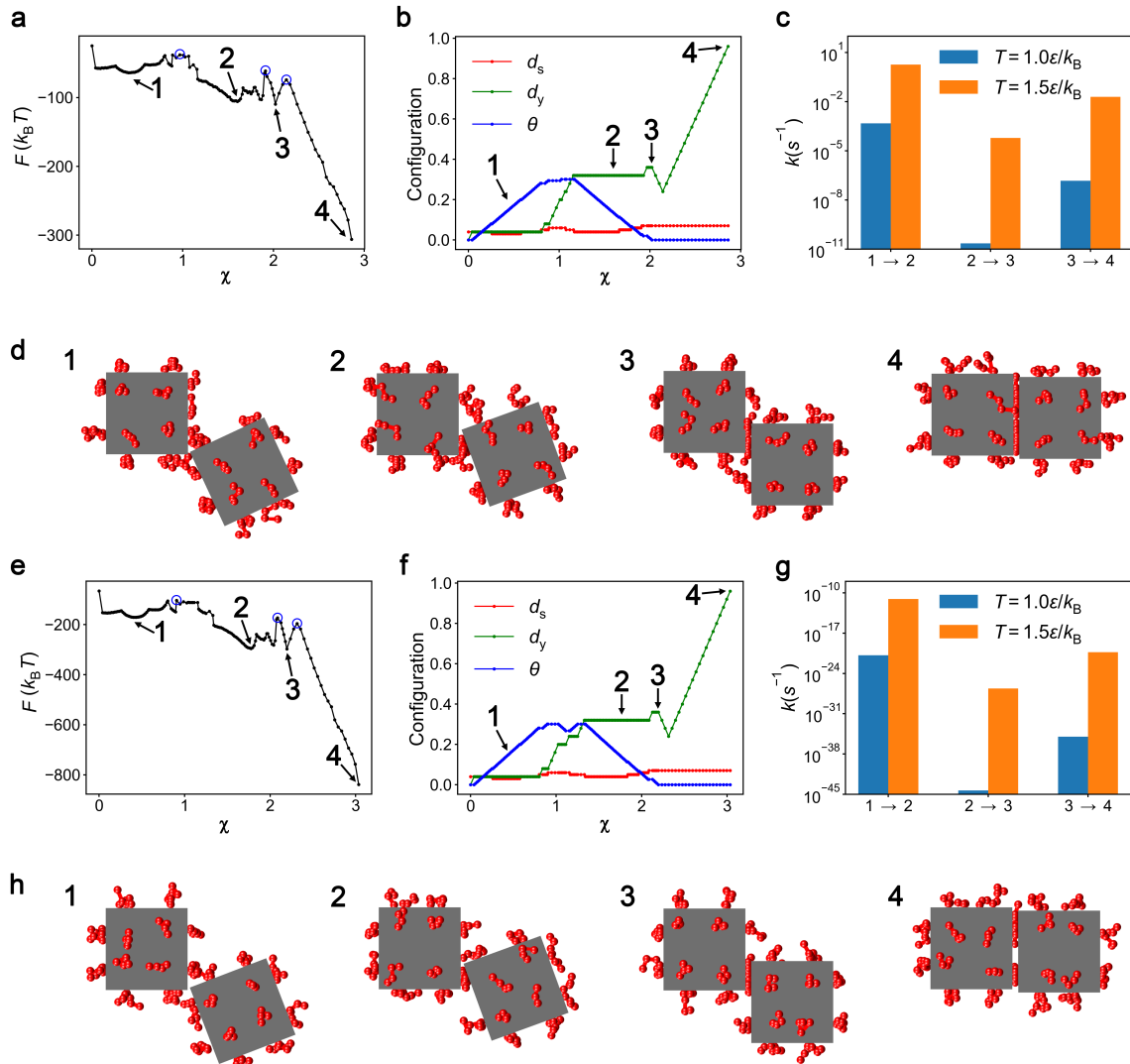


Figure 5: Assembly pathway and transition rates of nanocubes with rough surfaces. (a–h) Results corresponding to $[\sigma_{\text{lig}}, \varepsilon_{\text{cc}}] = [0.5\sigma, 0.75k_B T]$ (a–d) and $[0.5\sigma, 2k_B T]$ (e–h). (a, e) Free energy along the MFEP. Transition states between energy minima are marked by blue circles. (b, f) Nanocube configuration coordinates along the MFEP. (c, g) Transition rates between energy minima at the two specified temperatures. (d, h) Representative nanocube configurations at specific points along the MFEP indicated in (a, e) and (b, f).